ACS Photonics

Article

pubs.acs.org/journal/apchd5

Ultrabroad Bandwidth and Highly Sensitive Optical Ultrasonic Detector for Photoacoustic Imaging

Cheng Zhang, Tao Ling, Sung-Liang Chen, and L. Jay Guo*

Department of Electrical Engineering and Computer Science, University of Michigan, Ann Arbor, Michigan 48109, United States

Supporting Information

ABSTRACT: We demonstrate an ultrasonic detector with unprecedented broad bandwidth and high sensitivity, based on an imprinted polymer optical microring. It has an acoustic response of up to 350 MHz at −3 dB and noise-limited detectable pressure as low as 105 Pa in this frequency range. Application of such a detector in photoacoustic imaging leads to improved axial resolving ability compared with using the conventional ultrasound detector, and sub-3 μm axial resolution is achieved, which is more than a 2-fold improvement with respect to the reported record. The device's miniaturized cavity height guarantees its broadband response, and at the same time, its high optical quality factor ensures the detection sensitivity. Our work suggests that the polymer-based miniature microring resonator works as a high-performance ultrasound detector and has potential for acquiring volumetric photoacoustic images with cellular/subcellular resolution in three dimensions.

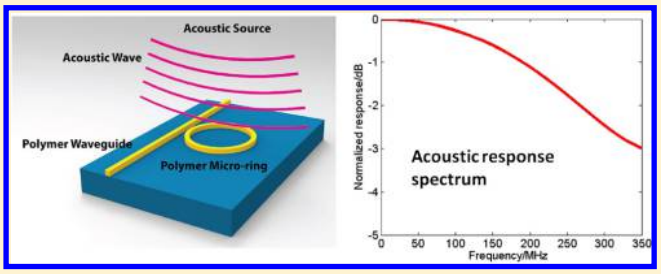

KEYWORDS: *broadband ultrasound detector, microring resonator, photoacoustic imaging, axial resolution*

Photoacoustic imaging (PAI), an elegant combination of light and sound, has been employed in such areas as laser ultrasound inspection,[1−4] photoacoustic microscopy/tomography,[5,6] and more recently pulsed THz detection and imaging.[7] A short laser pulse is used to illuminate light-absorbing objects, and ultrasound signals are generated via thermal-elastic expansion.[8] The signals are then collected by ultrasound detectors and used for image construction[9,10] or qualitative analysis.[11,12] Spatial resolution is one of the key parameters in PAI, in both lateral and axial dimensions. The existing PAI systems have demonstrated lateral resolution comparable to optical microscopy on the micro- or even submicrometer[13−16] scale by fine optical focusing. In sharp contrast, the axial resolution remains around 15−20 μm,[17,18] similar to that of high-frequency ultrasound imaging and more than 1 order of magnitude worse than the lateral spot size. The resultant asymmetric and severely distorted minimum voxel has a detrimental effect on the 3D imaging capability of PAI. The axial resolution is essentially determined by the sharpness of the detected acoustic pulse and can be described by the equation $R = 0.88C/BW$,[19] where R is the axial resolution, C the sound speed, and BW the detector fwhm bandwidth. Since C is a constant in most soft biological tissue, R is primarily determined by the detector's bandwidth.

Conventional ultrasonic transducers almost exclusively use piezoelectric material, either inorganic (e.g., piezoceramic materials)[20,21] or organic (e.g., polyvinyldenefluoride, PVDF).[22] Piezoelectric transducers are usually operated over a band of frequencies centered at their resonance where the thickness of the piezoelectric crystal equals half of the wavelength. Thus, high-frequency transducers require thin crystals, which results in demanding fabrication challenges and robustness issues from the fragile films.[23] Moreover, a broad bandwidth covering from nearly dc to very high frequencies is essential to subsequent faithful image reconstructions,[24] but this is not easily obtainable with a single piezoelectric transducer due to this resonant effect. To overcome such limitations, multiband photoacoustic imaging is developed, where multiple ultrasound detectors with different central frequencies are used to collect signals from the corresponding bands in a broad frequency range.[25,26] As an alternative to the finite bandwidth limitation on the detector side, researchers have obtained a 7.6 μm axial resolution with a commercial 125 MHz ultrasound transducer by applying a deconvolution method.[19] However, this method is sensitive to noise and therefore has limited applications. Another approach is to apply slow-sound silicone oil around the imaging target to improve the axial resolution,[27] but the biological compatibility of silicone oil needs to be further evaluated.

Ultrasound detection by optical methods is a promising field, where a structure with certain optical resonances is employed and its resonant behavior could be modulated by ultrasound waves. One popular optical ultrasound detector is the Fabry−Perot polymer film transducer.[28−30] Its cavity length is typically 25−50 μm in order to provide enough finesse (sensitivity), which limits the bandwidth to tens of MHz. Shelton et al. reported a novel approach to use optical nonlinearities to confine the spatial resolution in both lateral and axial dimensions and demonstrated an axial resolution of 6 μm.[31] But this technique uses a

Received: May 12, 2014
Published: October 20, 2014

   dx.doi.org/10.1021/ph500159g | *ACS Photonics* 2014, 1, 1093−1098

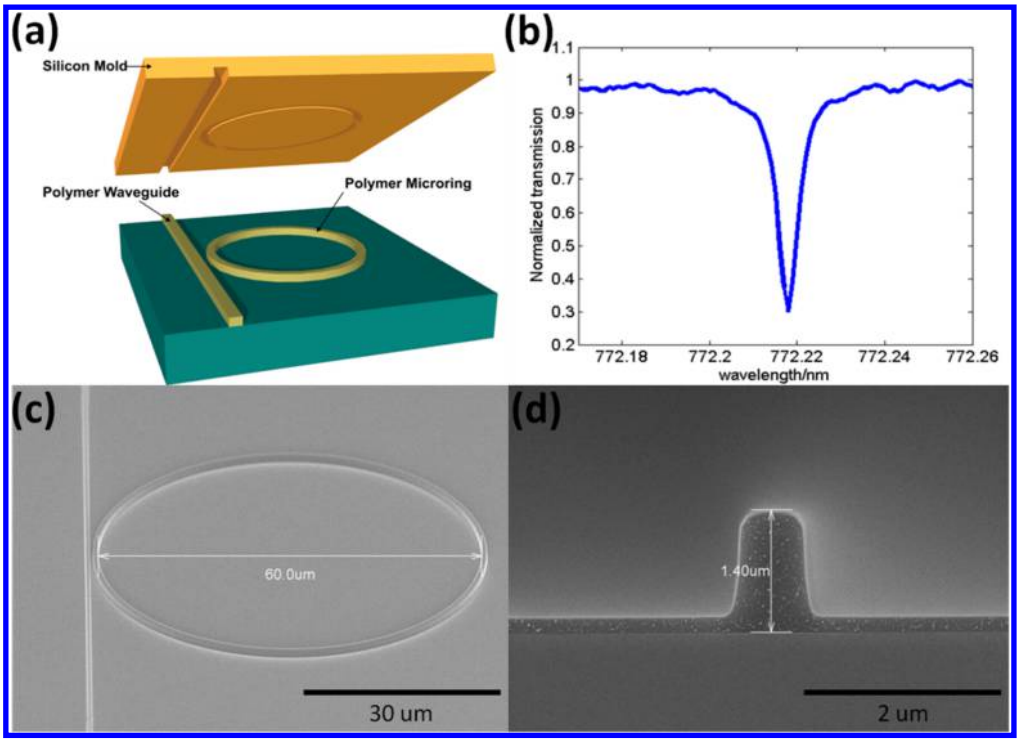

Figure 1. (a) Polymer ring fabrication schematic by nanoimprinting lithography. (b) Optical transmission spectrum of the polymer microring resonator. The resonance fwhm is ~6 pm. (c) Angle view scanning electron microscope (SEM) of the microring with a diameter of 60 μm. (d) Side view SEM picture of the ring with height of 1.4 μm.

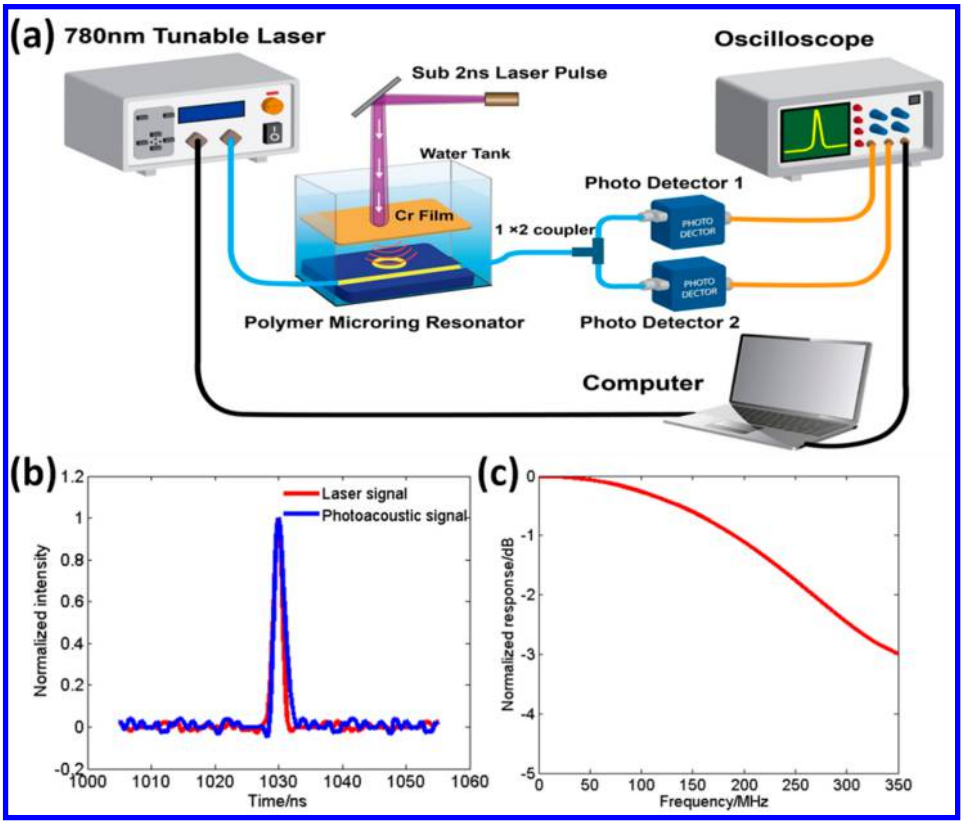

Figure 2. (a) Experimental setup to determine the bandwidth of the ring resonator. (b) Experimentally measured time domain laser signal (fwhm = 1.5 ns) and photoacoustic signal (fwhm = 1.8 ns). (c) Frequency domain microring response spectrum. The ring has a −3 dB bandwidth at 350 MHz.

complicated setup and has issues with the difficulty of miniaturization, limited imaging speed, and potential tissue damage.

Apart from bandwidth, detector sensitivity is another important parameter to consider. Since ultrasound attenuation is proportional to the square of frequency, the high-frequency

dx.doi.org/10.1021/ph500159g | ACS Photonics 2014, 1, 1093−1098

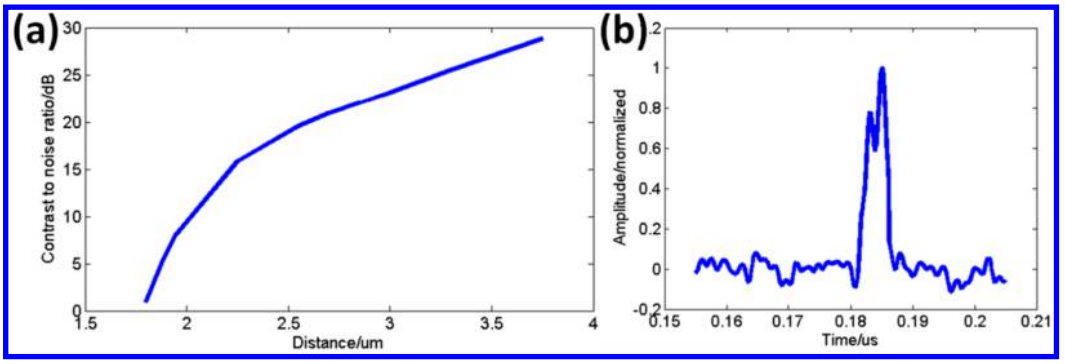

Figure 3. (a) Contrast to noise ratio (CNR) as a function of the delay distance. It reaches 6 dB at 1.9 μm (axial resolution estimation). (b) Two close Cr films with 1.9 ns separation in time domain, which is a direct experimental demonstration of the superhigh axial resolution (2.85 um).

component attenuates strongly with distance; for example, a 300 MHz acoustic wave attenuates at a rate of ~20 dB/mm in water and ~80 dB/mm in tissue.[13] Noise level increases proportionally with bandwidth at the same time. Therefore, in order to collect high-frequency photoacoustic signal effectively, a sensitive ultrasound detector is necessary.

In this work, we demonstrate an ultrasound detector based on polymer microring resonators with an ultrabroad bandwidth response from dc to ~350 MHz at −3 dB and an ultralow noise equivalent pressure (NEP) of 105 Pa over 350 MHz. The microring has a high quality factor on the order of 10^5, and such sharp resonance lays the foundation for sensitive acoustic detection. The minimized thickness of the microring waveguide is responsible for its ultrabroad bandwidth frequency response. An unprecedented sub-3 μm axial resolution is demonstrated experimentally by imaging two closely spaced chromium films. Our study proves that a polymer microring resonator is a high-performance ultrasound detector for photoacoustic imaging with ultrabroad bandwidth and high sensitivity.

RESULTS AND DISCUSSION

The polymer microring was fabricated by nanoimprinting of polystyrene (PS) film using a silicon mold (Figure 1a). The imprinting process simplifies fabrication, increases throughput, and improves reproducibility.[32] Details of the fabrication process can be found in the Supporting Information. The device consists of a ring resonator coupled with a bus waveguide. The ring has a diameter of 60 μm and height of 1.4 μm (Figure 1c and d). Resonant dips in the transmission spectrum occur when round-trip phase delay in the ring equals multiples of 2π. Figure 1b shows the measured optical transmission spectrum from the device. It has a resonance bandwidth of 6 pm, corresponding to a quality factor (Q factor) of 1.3×10^5. When the probing laser wavelength is fixed at the sharpest slope of the ring resonance curve, the incoming ultrasound signal can be recorded by the modulated output power from the microring resonator due to the resonance shift.

Ultrabroad Bandwidth and High Sensitivity. The experimental setup for investigating the device acoustic bandwidth is shown in Figure 2a. A continuous-wave (CW) 780 nm tunable laser (TLB-6312, New Focus) was fiber coupled into the device's input waveguide, and its output power was collected by a multimode fiber, which connected to a 1×2 coupler with 90:10 split ratio (FCMM50-90A-FC, Thorlabs). The outputs of the coupler were detected by two photodetectors and finally recorded by a digital oscilloscope (DSO7054A, Agilent). To lock the probing wavelength at the sharp slope of the ring resonance spectrum, output from the 10% channel of the coupler was monitored (1601, New Focus) and used for feedback control of the tunable laser, while the remaining 90% output was collected by a high-speed avalanche photodetector (APD210, Menlo Systems) and used for photoacoustic signal detection. The reason to collect as much output power as possible for photoacoustic detection is because the detection sensitivity is usually proportional to the probing optical power.[33] The device was immersed in deionized (DI) water, which served as both the top cladding of the microring and the coupling medium for the ultrasonic propagation. To determine the intrinsic bandwidth of the microring resonator, a narrow (broadband) acoustic pulse was needed. This was accomplished by photoacoustic signal generation, where a 1.5 ns pulse duration, 337 nm laser pulse (GL-3300, Photon Technology International) was used to illuminate a 200 nm thick chromium (Cr) film with ~4 mm spot size. In the case where the laser pulse duration is far longer than the acoustic transient time across the absorber, the generated photoacoustic signal essentially duplicates the incident laser pulse in the time domain.[34]

Figure 2b shows the time domain laser pulse and the photoacoustic signal detected by the microring, using the same high-speed photodetector. The full width half-maximum (fwhm) of the laser is 1.5 ns, and that of the photoacoustic signal is 1.8 ns. The photoacoustic signal was generated from a single laser pulse without any averaging. A ~20 μm water gap between the Cr film and the microring resonator was determined through the propagation time of the generated acoustic signal. The frequency response of the microring detector is plotted in Figure 2c, where the water acoustic attenuation compensation is taken into account. As can be seen, a flat response stretching from dc to ~350 MHz at −3 dB (0.707) was obtained. Such a wideband and flat spectral characteristic can tremendously enhance the axial resolution in photoacoustic imaging, as shown later. Detailed calculation of the frequency response is described in the Supporting Information.

The detector's acoustic sensitivity was calibrated using the same setup, but a precalibrated 20 MHz unfocused transducer (V316, Panametrics NDT) replaced the Cr film as the acoustic source. It was driven by a 2 V peak-to-peak one-cycle 20 MHz sinusoidal wave with an output peak pressure of 6 KPa. The device produced an output peak voltage of 120.3 mV without any averaging, corresponding to a sensitivity of 20.05 mV/KPa. The RMS noise level is 2.1 mV over the 1−350 MHz, leading to a NEP of 105 Pa. To our knowledge, this is the first time that low noise equivalent detectable pressure with a broad bandwidth of up to 350 MHz has been achieved. Further reduction of the NEP

dx.doi.org/10.1021/ph500159g | ACS Photonics 2014, 1, 1093−1098

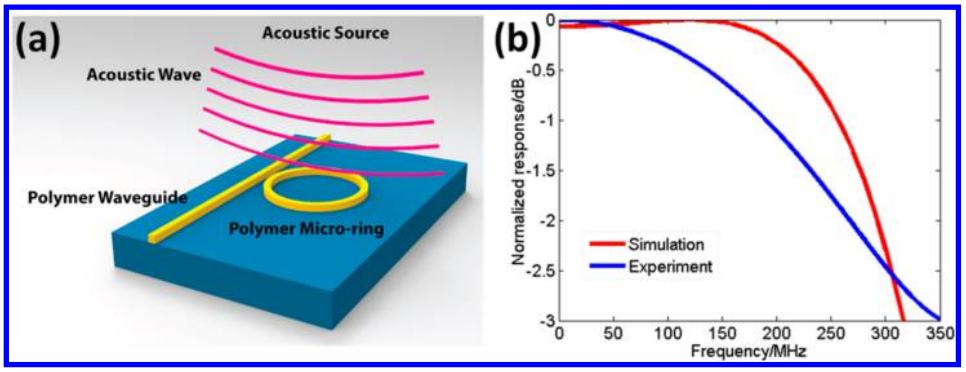

Figure 4. (a) Schematic drawing of the ring working as an acoustic resonator. (b) Simulated (red) and measured (blue) detector frequency response curves.

is possible by increasing the device Q factor, using higher probe laser power, and increasing the photodetector gain with low-noise base.

Sub-3 μm Axial Resolution. In Figure 2b, the measured photoacoustic signal has a fwhm of 1.8 ns. Considering the sound speed of 1500 m/s in tissue, this translates to a 2.7 μm axial resolution. Since the photoacoustic signals from objects at different locations add to each other in amplitude, objects with a separation less than 2.7 μm could still be distinguished. The system axial resolution could be estimated by shifting and summing the amplitude of two photoacoustic signals detected at a certain time interval and checking if the peaks can be distinguished (i.e., Rayleigh criterion). Zhang et al. define the difference in the signal envelope between the smaller of the two peaks and the valley as the contrast, and the contrast-to-noise ratio (CNR) decreases as the distance between the two signals is reduced.[19] The axial resolution is determined when the CNR reaches 6 dB. Using this method, we plot the CNR as a function of shift distance (Figure 3a), based on the detected photoacoustic signal in Figure 2b. The CNR reaches 6 dB with a separation of 1.9 μm, showing the potential of <2 μm axial resolution in photoacoustic imaging using the microring detector.

As an experimental demonstration, we replaced the single Cr film with two Cr films separated by a thin SU8 spacer. The Cr films are 40 and 160 nm thick, respectively, and the SU8 layer is about 5.9 μm. The films are deposited on a polyethylene terephtalate (PET) substrate, which has matched acoustic impedance with water.[27] No reflected acoustic wave from the substrate was observed in the experiment. The detected signal is shown in Figure 3b. Clearly two peaks can be distinguished with 1.9 ns separation and a CNR of 15 dB. A 1.9 ns time domain gap directly translates to 2.85 μm axial resolution in biological tissue (sound velocity 1500 m/s in tissues), consistent with the previous estimation based on the pulse width of the photoacoustic signal detected by the microring. This value is about a 2-fold improvement over the most recent reported results,[27,31] but without any signal processing or sample treatment. An initial experiment using the microring in a photoacoustic microscopy system also shows improved axial resolution as compared with a traditional transducer.[35] A more comprehensive study is currently under way.

Theoretical Analysis on the Frequency Response. First of all, the detector acoustic response bandwidth is limited by the cavity optical bandwidth, which is determined by the inverse photon lifetime in the cavity (ν/Q),[36] where ν is the operating frequency and Q the quality factor. This upper frequency limit, calculated to be ~18 GHz in the polymer microring case, is far beyond the frequency range for PAI (a few hundred MHz). From the acoustic interaction point of view, the microring resonator is modeled as a vertical acoustic Fabry–Perot (FP) cavity for the incident acoustic pulse.[37] The active region is the polystyrene waveguide core bounded by the water and the silicon dioxide (SiO_2) substrate, as shown in Figure 4a. The microring height is 1.4 μm. In this acoustic cavity, due to the smaller/comparable lateral size of the polystyrene waveguide to the ultrasound wavelength, the acoustic scattering effect cannot be neglected. For estimation, plane wave propagation inside the polystyrene waveguide is assumed. The incoming pressure partially transmits into this FP cavity and bounces back and forth between the two boundaries. Similar to an optical FP cavity, the cavity length of this acoustic FP roughly determines its response bandwidth. The amplitude of the accumulated acoustic field inside the PS waveguide can be calculated as a function of frequency. The greater the acoustic field accumulation, the stronger it would influence the PS waveguide property and the ring resonance behavior. It is worth noting that the distribution of optical field intensity inside the core of the microring optical waveguide is not uniform. For the fundamental optical mode, the field has high intensity in the center and low intensity near the boundaries. Therefore, for more accurate evaluation, the optical field distribution in the PS core was taken into account as a weighting factor in calculating the acoustic field accumulation's effect on the PS waveguide property. The detailed procedures used to analyze the frequency response are listed in the Supporting Information. The simulated frequency response is plotted in Figure 4b. Its −3 dB bandwidth is ~315 MHz, which agrees with the experimental result, although some differences between the two curves are observed. The discrepancy can be attributed to factors such as the plane wave approximation we used and how the optical field distribution is taken into account, as well as material parameters used in the simulation. Further investigation is currently under way.

Discussion. In the planar Fabry–Perot polymer film ultrasound detector case, the film thickness is typically chosen as 25–50 μm in order to guarantee high finesse (thus high sensitivity), which limits its bandwidth to tens of MHz based on a similar analysis discussed above. By sharp contrast, the microring resonator is able to maintain its high Q factor (high sensitivity) and broad bandwidth simultaneously. Therefore, it possesses both broad bandwidth and low NEP. The microring is an ideal detector for photoacoustic tomography, where objects of different sizes generate photoacoustic signals at different central frequencies.[38] The microring could effectively collect all signals as a single element, alleviating the complexity of employing

dx.doi.org/10.1021/ph500159g | ACS Photonics 2014, 1, 1093–1098

multiple detectors such as in multiband photoacoustic tomography. Therefore, the polymer-based miniature size microring resonance structure provides an advantageous approach for both broadband and sensitive ultrasound detection.

CONCLUSION

We have demonstrated an ultrabroad bandwidth and highly sensitive acoustic detector using polymer microring resonators. It has a flat frequency response stretching from dc to a −3 dB bandwidth up to 350 MHz. At the same time, the noise equivalent detectable pressure is as low as 105 Pa in this broad bandwidth. Such ultrabroad frequency response and unprecedented sensitivity make it an ideal detector in high-resolution photoacoustic imaging. Application of such a broadband detector in photoacoustic imaging system leads to improved axial resolving ability, and sub-3 μm axial resolution is experimentally demonstrated without any sample treatment or signal processing, leading to a 2-fold improvement over the reported record. The device's miniaturized cavity height guarantees its broadband response, and at the same time, its high optical quality factor ensures the detection sensitivity. Our study shows the polymer microring resonator is a promising detector for applications in photoacoustic imaging with its ultrabroad bandwidth and high sensitivity.

ASSOCIATED CONTENT

Supporting Information

Device fabrication; bandwidth calculation; detector frequency response extrapolation; bandwidth simulation. This material is available free of charge via the Internet at http://pubs.acs.org.

AUTHOR INFORMATION

Corresponding Author

*E-mail: guo@umich.edu.

Notes

The authors declare no competing financial interest.

ACKNOWLEDGMENTS

This work is supported by the National Science Foundation (DBI-1256001). We would like to acknowledge the technical support from Lurie Nanofabrication Facility (LNF) at University of Michigan. C.Z. acknowledges the useful discussion with Zeyu Pan on the waveguide simulation and thanks Elizabeth C. F. Dreyer and Qiaochu Li for linguistic revisions.

REFERENCES

(1) Wang, H.-C.; Fleming, S.; Lee, Y.-C.; Swain, M.; Law, S.; Xue, J. Laser ultrasonic evaluation of human dental enamel during remineralization treatment. *Biomed. Opt. Express* **2011**, *2*, 345−355.

(2) Balogun, O.; Huber, R.; Chinn, D.; Spicer, J. B. Laser ultrasonic inspection of the microstructural state of thin metal foils. *J. Acoust. Soc. Am.* **2009**, *125*, 1437−1443.

(3) Mezil, S.; Chigarev, N.; Tournat, V.; Gusev, V. All-optical probing of the nonlinear acoustics of a crack. *Opt. Lett.* **2011**, *36*, 3449−3451.

(4) Sridhar, K., Theory and Applications of Laser-Ultrasonic Techniques. In *Ultrasonic Nondestructive Evaluation*; CRC Press: Boca Raton, FL, 2003.

(5) Xu, M.; Wang, L. V. Photoacoustic imaging in biomedicine. *Rev. Sci. Instrum.* **2006**, *77*, 041101.

(6) Wang, L. V.; Hu, S. Photoacoustic tomography: in vivo imaging from organelles to organs. *Science* **2012**, *335*, 1458−1462.

(7) Chen, S.-L.; Chang, Y.-C.; Zhang, C.; Ok, J. G.; Ling, T.; Mihnev, M. T.; Norris, T. B.; Guo, L. J. Efficient real-time detection of terahertz pulse radiation based on photoacoustic conversion by carbon nanotube nanocomposite. *Nat. Photonics* **2014**, 537−542.

(8) Gusev, V. E.; Karabutov, A. A. *Laser Optoacoustics*; American Institute of Physics: New York, 1993; pp xvii, 271.

(9) Chen, S.-L.; Sheng-Wen, H.; Tao, L.; Ashkenazi, S.; Guo, L. J. Polymer microring resonators for high-sensitivity and wideband photoacoustic imaging. *IEEE Trans. Ultrason. Ferroelectr. Freq. Control* **2009**, *56*, 2482−2491.

(10) Xiang, L.; Wang, B.; Ji, L.; Jiang, H. 4-D photoacoustic tomography. *Sci. Rep.* **2013**, *3*, 1113.

(11) Strohm, E. M.; Berndl, E. S. L.; Kolios; Michael, C. Probing red blood cell morphology using high-frequency photoacoustics. *Biophys. J.* **2013**, *105*, 59−67.

(12) Xu, G.; Meng, Z.-X.; Lin, J. D.; Yuan, J.; Carson, P. L.; Joshi, B.; Wang, X. The functional pitch of an organ: quantification of tissue texture with photoacoustic spectrum analysis. *Radiology* **2014**, *271*, 130777.

(13) Maslov, K.; Zhang, H. F.; Hu, S.; Wang, L. V. Optical-resolution photoacoustic microscopy for in vivo imaging of single capillaries. *Opt. Lett.* **2008**, *33*, 929−931.

(14) Zhang, C.; Maslov, K.; Hu, S.; Chen, R.; Zhou, Q.; Shung, K. K.; Wang, L. V. Reflection-mode submicron-resolution in vivo photoacoustic microscopy. *J. Biomed. Opt.* **2012**, *17*, 0205011−0205014.

(15) Zhang, C.; Maslov, K.; Wang, L. V. Subwavelength-resolution label-free photoacoustic microscopy of optical absorption in vivo. *Opt. Lett.* **2010**, *35*, 3195−3197.

(16) Xie, Z.; Jiao, S.; Zhang, H. F.; Puliafito, C. A. Laser-scanning optical-resolution photoacoustic microscopy. *Opt. Lett.* **2009**, *34*, 1771−1773.

(17) Wang, L.; Maslov, K.; Yao, J.; Rao, B.; Wang, L. V. Fast voice-coil scanning optical-resolution photoacoustic microscopy. *Opt. Lett.* **2011**, *36*, 139−141.

(18) Yu, W.; Maslov, K.; Chulhong, K.; Song, H.; Wang, L. V. Integrated Photoacoustic and Fluorescence Confocal Microscopy. *IEEE Trans. Biomed. Eng.* **2010**, *57*, 2576−2578.

(19) Zhang, C.; Maslov, K.; Yao, J.; Wang, L. V. In vivo photoacoustic microscopy with 7.6 μm axial resolution using a commercial 125-MHz ultrasonic transducer. *J. Biomed. Opt.* **2012**, *17*, 116016−116016.

(20) Hunt, J. W.; Arditi, M.; Foster, F. S. Ultrasound transducers for pulse-echo medical imaging. *IEEE Trans. Biomed. Eng.* **1983**, *30*, 453−481.

(21) Davidsen, R. E.; Smith, S. W. Two-dimensional arrays for medical ultrasound using multilayer flexible circuit interconnection. *IEEE Trans. Ultrason. Ferroelectr. Freq. Control* **1998**, *45*, 338−348.

(22) Foster, F. S.; Harasiewicz, K. A.; Sherar, M. D. A history of medical and biological imaging with polyvinylidene fluoride (PVDF) transducers. *IEEE Trans. Ultrason. Ferroelectr. Freq. Control* **2000**, *47*, 1363−1371.

(23) Oraevsky, A. A.; Karabutov, A. A. Ultimate sensitivity of time-resolved optoacoustic detection. *Proc. SPIE* **2000**, *3916*, 228−239.

(24) Minghua, X.; Yuan, X.; Wang, L. V. Time-domain reconstruction algorithms and numerical simulations for thermoacoustic tomography in various geometries. *IEEE Trans. Biomed. Eng.* **2003**, *50*, 1086−1099.

(25) Geng, K.; Xueding, W.; George, S.; Lihong, V. W. Multiple-bandwidth photoacoustic tomography. *Phys. Med. Biol.* **2004**, *49*, 1329.

(26) Gateau, J.; Chekkoury, A.; Ntziachristos, V. Ultra-wideband three-dimensional optoacoustic tomography. *Opt. Lett.* **2013**, *38*, 4671−4674.

(27) Zhang, C.; Zhou, Y.; Li, C.; Wang, L. V. Slow-sound photoacoustic microscopy. *Appl. Phys. Lett.* **2013**, *102*, 163702.

(28) Zhang, E.; Laufer, J.; Beard, P. Backward-mode multiwavelength photoacoustic scanner using a planar Fabry-Perot polymer film ultrasound sensor for high-resolution three-dimensional imaging of biological tissues. *Appl. Opt.* **2008**, *47*, 561−577.

(29) Zhang, E.; Beard, P. Broadband ultrasound field mapping system using a wavelength tuned, optically scanned focused laser beam to address a Fabry Perot polymer film sensor. *IEEE Trans. Ultrason. Ferroelectr. Freq. Control* **2006**, *53*, 1330−1338.

(30) Hajireza, P.; Krause, K.; Brett, M.; Zemp, R. Glancing angle deposited nanostructured film Fabry-Perot etalons for optical detection of ultrasound. *Opt. Express* **2013**, *21*, 6391−6400.
(31) Shelton, R. L.; Applegate, B. E. Ultrahigh resolution photoacoustic microscopy via transient absorption. *Biomed. Opt. Express* **2010**, *1*, 676−686.
(32) Guo, L. J. Nanoimprint lithography: methods and material requirements. *Adv. Mater.* **2007**, *19*, 495−513.
(33) Huang, S.-W.; Chen, S.-L.; Ling, T.; Maxwell, A.; O'Donnell, M.; Guo, L. J.; Ashkenazi, S. Low-noise wideband ultrasound detection using polymer microring resonators. *Appl. Phys. Lett.* **2008**, *92*, 193509.
(34) Diebold, G. J.; Sun, T.; Khan, M. I. Photoacoustic monopole radiation in one, two, and three dimensions. *Phys. Rev. Lett.* **1991**, *67*, 3384−3387.
(35) Xie, Z.; Tian, C.; Chen, S.-L.; Ling, T.; Zhang, C.; Guo, L. J.; Carson, P. L.; Wang, X. 3D high resolution photoacoustic imaging based on pure optical photoacoustic microscopy with microring resonator. *Proc. SPIE* **2014**, *8943*, 894314−894314−6.
(36) Armani, D. K.; Kippenberg, T. J.; Spillane, S. M.; Vahala, K. J. Ultra-high-Q toroid microcavity on a chip. *Nature* **2003**, *421*, 925−928.
(37) Beard, P. C.; Perennes, F.; Mills, T. N. Transduction mechanisms of the Fabry-Perot polymer film sensing concept for wideband ultrasound detection. *IEEE Trans. Ultrason. Ferroelectr. Freq. Control* **1999**, *46*, 1575−1582.
(38) Chen, S.-L.; Ling, T.; Guo, L. J. Low-noise small-size microring ultrasonic detectors for high-resolution photoacoustic imaging. *J. Biomed. Opt.* **2011**, *16*, 056001−056001−6.